Materials Science and Engineering C 30 (2010) 331–342

Contents lists available at ScienceDirect

Materials Science and Engineering C

journal homepage: www.elsevier.com/locate/msec

Review

Energy absorbent natural materials and bioinspired design strategies: A review

J. McKittrick [a,b,*], P.-Y. Chen [b], L. Tombolato [a], E.E. Novitskaya [b], M.W. Trim [c], G.A. Hirata [d], E.A. Olevsky [e], M.F. Horstemeyer [c], M.A. Meyers [a,b]

[a] Dept. of Mechanical and Aerospace Engineering, La Jolla, CA 92037, USA
[b] Materials Science and Engineering Program, La Jolla, CA 92037, USA
[c] Mechanical Engineering Department, Mississippi State University, Starkville, MS 39762, USA
[d] Center for Nanoscience and Nanotechnology, UNAM, Ensenada, Mexico
[e] Dept. of Mechanical Engineering, San Diego State University, San Diego, CA 92182, USA

ARTICLE INFO

Article history:
Received 15 September 2009
Received in revised form 24 December 2009
Accepted 14 January 2010
Available online 28 January 2010

Keywords:
Structural biological materials
Energy absorption
Bioinspired design

ABSTRACT

Some of the most remarkable materials in terms of energy absorption and impact resistance are not found through human processing but in nature. Solutions to the continuing problems of improved composite technologies may lie in replicating naturally occurring systems. In this review, we examine several mammalian structural materials: bones (bovine femur and elk antler), teeth and tusks from various taxa, horns from the desert big horn sheep, and equine hooves. We establish the relationships between structural and mechanical properties for these materials, with an emphasis on energy absorption mechanisms. We also identify the energy absorbing strategies utilized in these materials. Implementation of these bioinspired design strategies can serve as a basis for the design of new energy absorbent synthetic composite materials. Synthetic constituent materials arranged according to the principles outlined in this work will achieve the same synergistic effects as nature and no longer be confined to the limitations imposed by a mixture law.

Contents

1. Introduction

Biological structural materials show a wide range of function and form. Teeth and tusks have the same chemical composition and microstructure yet serve vastly different purposes. The same applies to bone and antler. Given that nature has optimized biological structural materials as functionally efficient configurations, examining these

* Corresponding author. Dept. of Mechanical and Aerospace Engineering, La Jolla, CA 92037, USA. Tel.: +1 858 534 5425; fax: +1 858 534 5698.
E-mail address: jmckittrick@ucsd.edu (J. McKittrick).

0928-4931/$ – see front matter © 2010 Elsevier B.V. All rights reserved.
doi:10.1016/j.msec.2010.01.011

natural materials and establishing the relationships between structure, function and properties is of great interest. A new paradigm for the fabrication of lightweight, impact resistant structures lies within the study of structural biological materials. These tissues are built under ambient conditions with only a few major elements (C, O, H, P, N, S, Ca, and Si). The similarities between structural biological materials such as mollusk shells, diatoms, sea sponges, teeth, tusks, bone, antlers, crab exoskeletons and insect cuticles are pronounced in that all structures are composites composed of a biopolymer (structural proteins such as collagen, keratin and elastin and polysaccharides such as cellulose and chitin) and a mineral phase (calcium carbonate, carbonated hydroxyapatite, or silica). Additionally, there is structural hierarchy that displays organization at all levels, from the nanoscale to the macroscale. The biopolymer imparts toughness and resilience while the biomineral increases hardness and stiffness.

These biological materials usually serve several purposes such as protection (mollusk shell, bones), defense and aggression (claws, teeth, tusks, horns, and antlers), support (bones, mollusk shell, and hooves) and mastication (teeth). There is a synergistic effect between the biopolymer and mineral phases — both are greatly dependent on the presence of the other to impart the multi-objective mechanical properties. This is illustrated in the Wegst–Ashby plot [1], which shows that the Young's modulus is low and toughness is high for biopolymers while the stiffness is high but toughness is low for the mineral phase. However, combining the two gives biological materials such as bone, teeth, antler and mollusk shells, toughness and stiffness values that are orders of magnitude higher than the pure mineral and pure biopolymer, respectively. From this observation, one can deduce that nature has no respect for the law of mixtures.

In order to understand structural biological materials, a few questions must be answered: What is (are) their function(s)? How are they used? And, what loading conditions are present? Bones provide structural support and protection of internal organs. The largest natural stresses are compressive in the long leg bones and vertebrae. Failure can occur by many modes: torsion, bending, shear, compression, impact and fatigue loading. Cancellous (spongy) bone appears in the skeleton where resistance to high impact loads is important — the skull, ribs, vertebrae and the head of the femur. They also ensure a higher flexural strength-to-weight ratio by forming the core of these bones, similar to sandwich panels. The multifunctional aspect of the cancellous bone must also be considered since it houses bone marrow and vascular channels. Antlers are only used in combat and therefore must be impact resistant and have high resistance to bending and shear deformation. Antlers are deciduous, being cast off after growing for roughly six months and are unlikely to fracture by fatigue cycling. An elk can run at speeds up to 11 m/s and typically weighs 320 kg with a kinetic energy associated with the impact of 19 kJ. The fracture resistance of antlers is high with only a few breakages observed in the wild [2]. The teeth must be able to bite and tear flesh and sustain high compressive loads. Tusks, which are long canine teeth that protrude from the mouth, are used for fighting and piercing. The horns from a big-horned sheep must be able to sustain large impact loads. The sheep do not shed their horns; they are a lifetime appendage. The average lifespan of a bighorn sheep is around 13 years; thus, the horns must be able to withstand repeated seasons of horn clashing without breakage. Hooves, found on ungulate mammals, transfer compressive loads to the skeleton, and in horses especially, undergo repeated high impact stresses.

Bioinspired materials are synthetic materials that are fabricated to mimic the structure and mechanical properties of biological structural materials. Instead of using the limited library of elements and compounds available in nature, the task lies in mimicking the natural materials using high strength, high toughness engineering materials. The bioinspired design effort first involves the search for biological solutions in design. For example, antlers and horns are known to be impact resistant. Thus, designs based on these microstructures could be stronger and tougher than their natural counterparts, because the components would be synthetic engineering materials and not biominerals and biopolymers. Determination of the mechanical properties and establishment of the relationship between the structure and function is the second step in the design of bioinspired materials. Finally, the application of engineering knowledge can be used to design new materials, using engineering ceramics, polymers and metals. However, establishing the structure–property relationships in the natural materials is the primary concern before tackling bioinspired materials designs.

In this review paper, we consider mammalian structural materials: bones (bovine femur and elk antler), teeth and tusks from various taxa, horns from the desert big horn sheep, and equine hooves. These biological materials are simultaneously strong, lightweight, able to sustain compressive loading, and are impact resistant. The questions are: (a) how are these biological materials arranged microstructurally and (b) is there is an underlying theme to these structures to make them so energy absorbent? Our hypothesis is that there must be a structural resemblance at some level, given that some of the functional requirements are similar. Our goal is to establish the relationships between structure and mechanical properties, in particular, energy absorption mechanisms. This will serve as a basis for the design of new energy absorbent synthetic materials.

2. Experimental

A number of different mechanical tests were performed to help quantify the structure–property relationships and identify microstructural features described in [3–8]. Cyclic compressive tests were conducted on cube samples of horn and demineralized antler in the longitudinal direction to obtain stress–strain hysteresis curves. A universal testing machine (Instron 3367 Dual Column Testing Systems, Instron, MA, USA) equipped with a 30 kN load cell was used. Specimens were tested at a strain rate of $1\times10^{-4}\,s^{-1}$. Demineralization of the antler was accomplished after soaking compact antler sections in HCl for a few days.

High strain rate compression tests were conducted using a split Hopkinson pressure bar (Kolsky) apparatus with the striker, incident, and transmitter bars all consisting of 7075-T651 aluminum 38.1 mm in diameter. The high strain rate specimens had a cylindrical geometry ($L=6.35$ mm, $d=12.7$ mm). The high strain rate compression data was analyzed using the DAVID software package, which compensates for the inherent dispersion of the wave and calculates the force and velocity at both faces of the specimen during the test to verify force equilibrium. Force equilibrium between the two faces of each specimen was validated. All strain rates were calculated as the best linear correlation of a strain versus time plot from a strain level of 0.02 to the end of the data.

3. Results, comparisons and discussion

3.1. Mineralized biological composites

3.1.1. Bone and antler

There are two types of bone: cancellous and compact. Cancellous (trabecular or spongy) bone is a highly porous, lamellar bone that is composed of interconnected platelets and rods and has a density of ~0.4 g/cm^3. This bone is surrounded by higher density compact bone (~2 g/cm^3), which is characterized by microstructural features called osteons. Osteons have concentric lamellae surrounding a main channel (blood vessel) that have alternating oriented collagen fibrils in the lamellae. The collagen fibrils are composed of tropocollagen molecules (~300 nm long, ~1.5 nm diameter), which are a triple helix of the collagen molecule. These fibrils are held together by other proteins and have the mineral phase dispersed between and around them. The mineral phase is a calcium phosphate, a form similar to hydroxyapatite ($Ca_{10}(PO_4)_6(OH)_2$), which is 4 nm thick and 30–

200 nm wide, and comprises 33–43 vol.% of skeletal bone [9]. Thus, bone is a composite on two levels — a collagen fiber-reinforced and mineral particulate-reinforced composite material. The hierarchical structure of bone is shown in Fig. 1, illustrating the collagen fibril and osteon arrangement. The other significant phase is water, which comprises ~15–25 vol.% [10]. Water is located in several regions: within the fibrils, between the fibrils (gaps) and between triple helix tropocollagen molecules [11]. Antler bone is less mineralized than skeletal bone, with a mineral content of 33 vol.% [7], and consequently has a lower Young's modulus but a higher toughness.

3.1.2. Tooth and tusk

The hierarchical structure of a tooth is shown in Fig. 2(a)–(c). Teeth and tusks among various taxa show surprising similarity. They are both composed of an outer thin enamel layer consisting of ~92 vol.% hydroxyapatite, 2 vol.% collagen and 6 vol.% water and a core (dentin) that is a composite of the mineral (~50 vol.%), collagen and other proteins (~30 vol.%) and water (~20 vol.%) [12]. Tubules extend perpendicularly from the pulp and are surrounded by the mineral phase. These tubules are filled with fluid when in the live animal. At the very center is the pulp and there is a vascular, nerve-containing core that connects to the body's main vascular system. Fig. 2(d) shows a cross-section of a human tooth along with Vickers hardness data across the cross-sectional area (perpendicular to the growth direction). The enamel has a hardness (~1.5 GPa) that is 3× higher than that of dentin. The enamel represents the highest mineralized biological material, and has a woven structure, shown in Fig. 2(b). The elastic modulus of enamel is characteristically 80 GPa [15]. The mineral is primarily located surrounding the ~1 μm diameter tubules. The tubule density varies between 4900 and 57,000 mm^{-2} increasing from the enamel region to the interior [15–18]. The Young's modulus of dentin is highest for the highly mineralized peritubular dentin and is lower for the less mineralized intertubular dentin [19]. Teeth and tusks have a widely varying function: tearing meat (great white and mako shark teeth), gnawing (rabbit teeth), fighting (warthog tusks) tearing fish (piranha), slicing fish (sawfish rostrum), biting and mastication (human teeth). Although there are functional differences, they nonetheless have structural (hard outer sheath mitigated by a soft but tough interior) and mechanical properties that are similar. Because the gradient in the porosity ranges from being lowest at the surface and increasing into the interior, there exists an inverse relation to the elastic modulus.

One important feature of the mineralized hard tissues is that the mineral phase is nanocrystalline. The Griffith equation relates the failure strength (σ_f) to the size of a surface flaw (a) by the following equation,

$$K_{Ic} = Y\sigma_f\sqrt{\pi a} \tag{1}$$

where Y is a geometrical constant, and K_{IC} is the plane strain fracture toughness. Hydroxyapatite and calcium carbonate have fracture toughness values of ~1 MPa√m. The tensile strengths for the abalone shell (170 MPa [8]) or bone (160 MPa [20]) can be applied to Eq. (1). Thus, one obtains critical flaw sizes of 35 μm and 40 μm for abalone and bone, respectively ($Y=1$, $K_{IC}=1$ MPa√m), which is much larger than the sizes of the minerals. This demonstrates that the failure of the composites is not through brittle fracture of the mineral phase. Indeed, it has been suggested by Imbeni et al. [14] that the critical structural elements are mesoscale features. Additionally, Gao et al. [21] pointed out that the shape of the mineral is important. As a rough estimate, the Young's modulus (E) of a composite is given by [21]:

$$\frac{1}{E} = \frac{4(1-\Phi)}{G_p\Phi^2\rho^2} + \frac{1}{\Phi E_m}, \tag{2}$$

where Φ is the volume fraction of the mineral phase, G_p is the shear modulus of the protein, ρ is the aspect ratio of the mineral, and E_m is the elastic modulus of the mineral. Eq. (2) indicates that the high modulus of the composite increases as the aspect ratio of the reinforcing phase increases. Nacre tiles ($\rho\sim20$) and hydroxyapatite ($\rho\sim7$) demonstrate the importance of a large aspect ratio and thus is a likely reason why equiaxed mineral particles are not observed in structural biological materials.

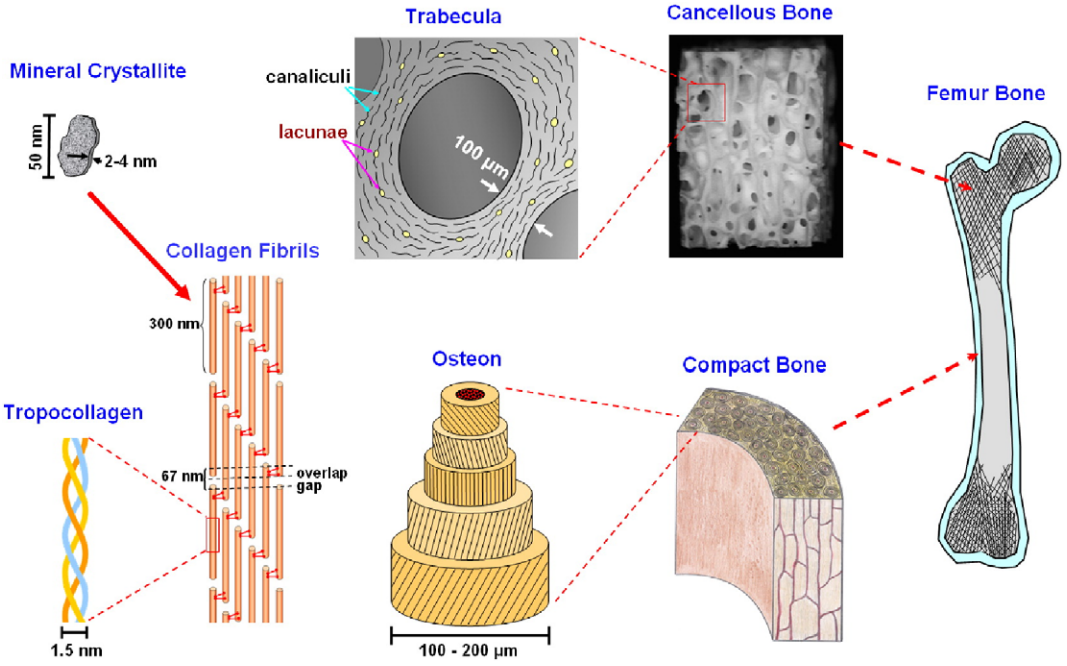

Fig. 1. Hierarchical structure of bone and antler.
Modified from Chen et al. [7].

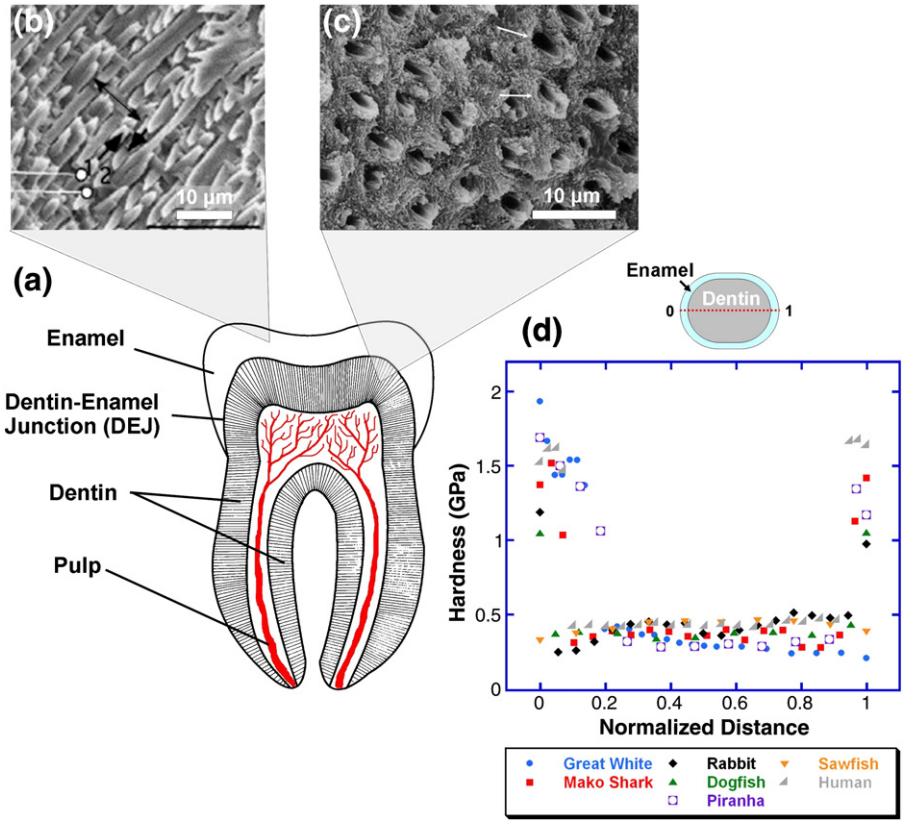

Fig. 2. Hierarchical structure of tooth. (a) Schematic drawing shows enamel, dentin–enamel junction, dentin, and pulp; (b) scanning electron micrograph of mouse tooth shows an etched image of mature enamel where the enamel rods weave past one another [13], (c) scanning electron micrograph of dentin [14], and (d) Vickers hardness number data across teeth for various taxa. The high values are for enamel and the lower values for dentin.
Adapted from Chen et al. [8].

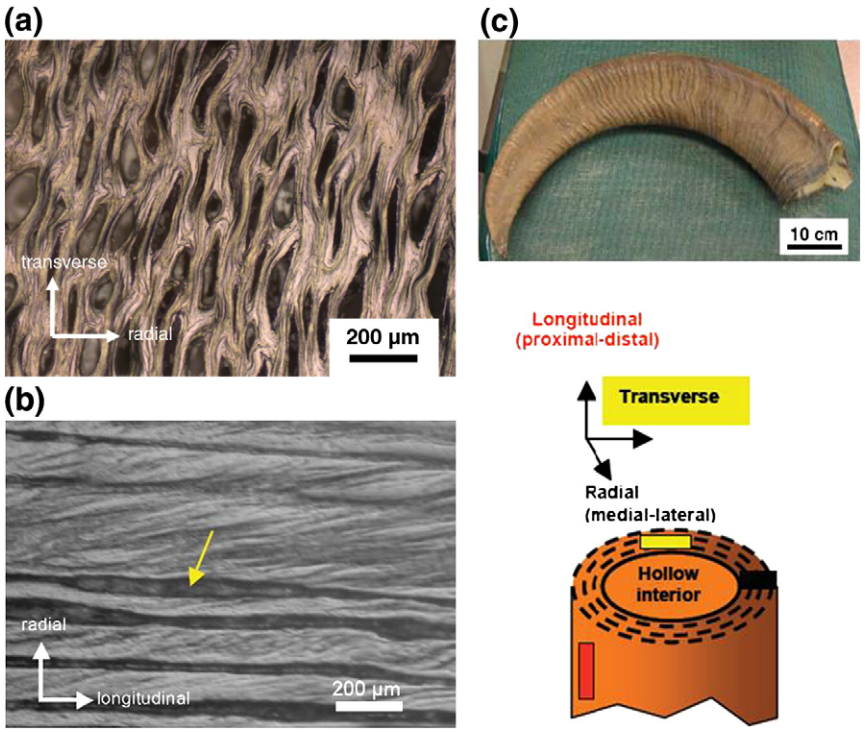

Fig. 3. Optical micrographs of ambient dried horn. (a) Cross-section showing the dark elliptical-shaped tubules, (b) longitudinal section showing the outline of the parallel tubules (arrow points to a tubule) and (c) orientation of the samples in the horn.
Taken from Tombolato et al. [3].

3.2. Non-mineralized biological composites

3.2.1. Horn

In most cases, horns comprise a keratin sheath, surrounding a core of cancellous bone, the single exception being rhinoceros horn, which does not have a bony core [22]. Horns, hooves, hair, furs, claws and fingernails are all made from keratin, which is a tough, fibrous structural protein. Horn is composed of α-keratin crystalline filaments embedded in an amorphous protein (mostly non-crystalline keratin) matrix [23]. Horn keratin has a lamellar structure (2–7 μm in thickness) stacked in the radial direction with tubules (~20 to 100 μm in diameter) dispersed between the lamellae, extending along the length of the horn (growth direction), as shown in Fig. 3 [3]. Optical micrographs of a cross-sections perpendicular and parallel to the growth directions are shown in Fig. 3. The tubules appear to extend continuously in the growth direction, as no terminal points were identified. The tubules are elliptically shaped and form small delaminated regions between the lamellae.

Kitchener and Vincent [23] found that the horn from a live animal had 20 wt.% water, yet the horn could be immersed in water to a saturated value of 40 wt.% water. This additional water was likely stored within the empty tubules and fully hydrated the amorphous keratin matrix. It appears that on the live animal, the tubules are void and only serve a mechanical purpose, similar to hooves (see below).

Fig. 4 shows the effect of strain rate on the stress–strain behavior where the horn was loaded in compression at quasi-static rates and also under high strain rates in the split Hopkinson bar. When the rams butt heads, the horns are loaded in the radial direction, which also provides more energy absorption than in the longitudinal direction. The Young's modulus, the yield strength and the toughness increase as the strain rate increases, which are typical behaviors of polymers. As the strain rate increases, the polymer chains do not have the time necessary to align and thus behave more as a polymer network. However, the strains to failure are tremendous, as much as 80%, which is an order of magnitude higher than in a typical network polymer. This is due to dissipative

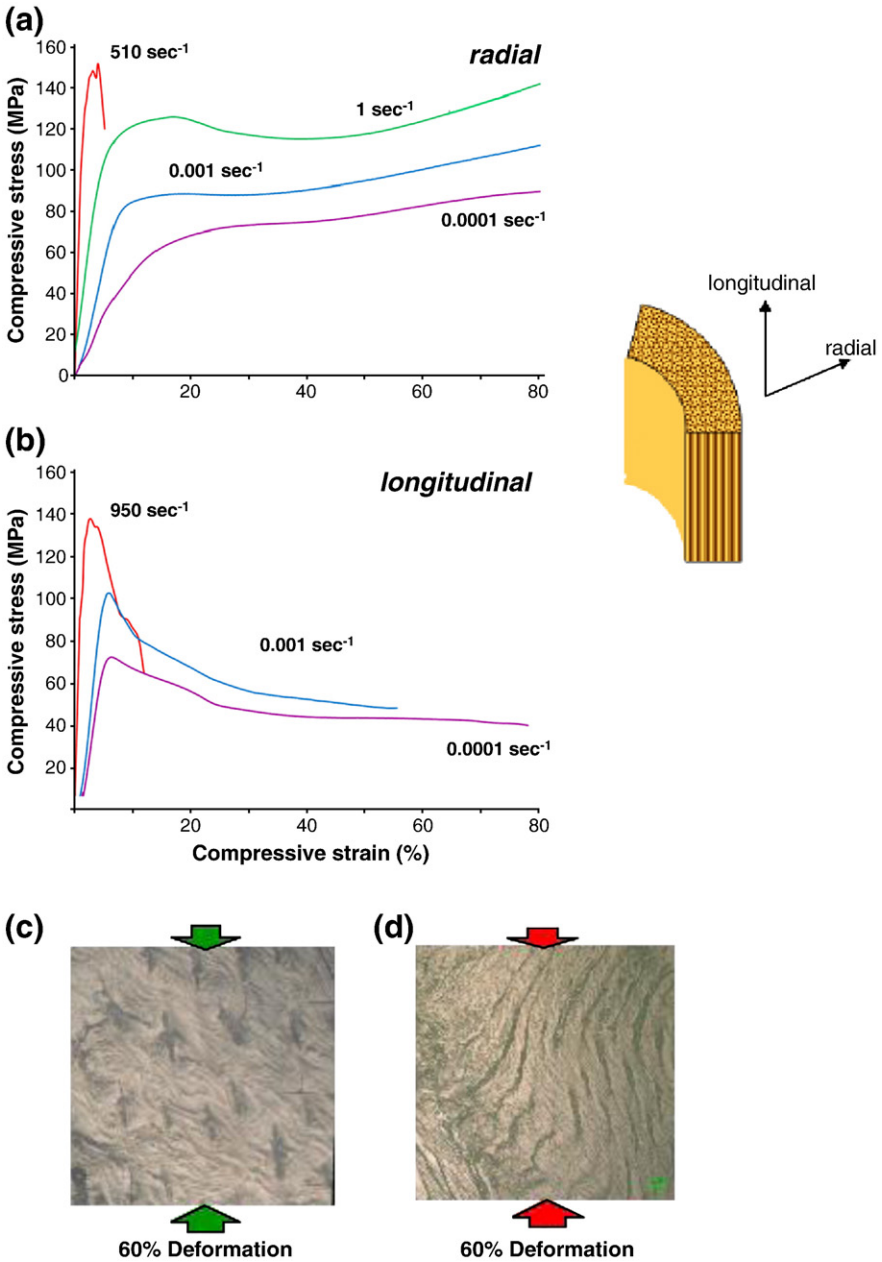

Fig. 4. Effect of strain rate on the compression stress–strain curve for big horn sheep horn in the (a) radial and (b) longitudinal directions. (c) Micrograph showing tubule collapse after a compressive load and (d) micrograph showing microbuckling of the lamellae. Adapted from Tombolato et al. [3].

microdeformation processes such as compression of the tubules (Fig. 4(c)). The longitudinal stress–strain behavior shows a higher Young's modulus and yield strength compared with the radial samples. This is due to the alignment of the lamellae, which extend in the longitudinal direction. However, the toughness is lower and the samples fail by microbuckling and delamination of the lamellae (Fig. 4(d)).

The problem of buckling of a thin laminated surface layer can be considered as a classical linear problem of buckling of a strip with fixed ends. Assuming plane strain, this critical delamination buckling stress is given by [24]:

$$\sigma_c = \frac{\pi^2 E}{2(1-\nu^2)}\left(\frac{h}{\ell}\right)^2 \tag{3}$$

where h is the thickness of the lamellae, ℓ is the length of the buckled region, E is the Young's modulus, and ν is the Poisson's ratio. For the case of horn with compressive loading parallel to the lamellae, $h/\ell = 1/20$, $E = 2.4$ GPa, and $\nu = 0.3$. Inserting these values into Eq. (3) gives a critical buckling stress of 23 MPa, which is lower than the plateau stress observed at quasi-static strain rates (Fig. 4). The observed stress is higher due to the microfibril ligaments bridging the lamellae, as discussed below. Interestingly, this type of microbuckling behavior has also been observed in abalone nacre [25].

The delamination energy (U_{del}) can be expressed by:

$$U_{del} = \frac{2}{9}\left(\frac{\tau^2}{E}\right)\left(\frac{wL^3}{t}\right), \tag{4}$$

where τ is the interlaminar shear strength, w is the width of the plate, L is the length of the plate and t is the thickness of the lamellae. This equation indicates the delamination energy parabolic function of the interlaminar shear strength. In horn, keratin fibril bundles are not only found aligned in the longitudinal (growth) direction, but also extend perpendicularly, attaching one lamella to the adjacent one, as shown in the TEM micrographs in Fig. 5. Due to the thinness of the sample (70 nm) and the desiccating environment in the microscope, the lamellae separated forming the white, elliptically shaped regions in the micrograph in Fig. 5(a). Stretching across these delaminated regions are strongly diffracting, crystalline keratin fibril bundles that are ~40 nm in diameter. These fibrils serve to strengthen the interface between the lamellae and increase the interlaminar shear strength, τ, thereby increasing U_{del} (Eq. (4)). In Fig. 5(b), numerous bundles are observed that connect two lamellae and Fig. 5(c) images a single bundle, showing the crystalline fibrils embedded in an amorphous matrix. In addition, a low stiffness and thin lamellae increase the delamination energy, which is the case for horn. The lamellae are thin (2–7 μm), whereas synthetic laminates are in the macroscopic range and the stiffness is low (2.4 GPa) compared to synthetic laminates. The fibril bundles stitch the lamellae together that provide sliding resistance and increasing the interlaminar shear strength. An increase in the interlaminar shear strength has been observed in synthetic laminates, where cross-stitching of laminates of graphite fiber-reinforced polymers significantly increased the delamination resistance by up to an order of magnitude [26]. However, cross-stitching reduced the ultimate strength, due to damage to the fibers in the laminate during the stitching [27], which is not the case for the horn. Thus, in comparison to synthetic laminates, the horn structure is superior.

The rhinoceros horn is another example of a tubule-containing keratin material. The rhino rubs its horn on trees and stones to keep it sharp and it can be up to 30 cm in length. It has a circular lamellar structure composed of keratin fibers, illustrated in Fig. 6(a) [22]. The rhinoceros will use its horn to push and spar with each other and puncture adversaries, thus it too must be sturdy and resistant to fracture.

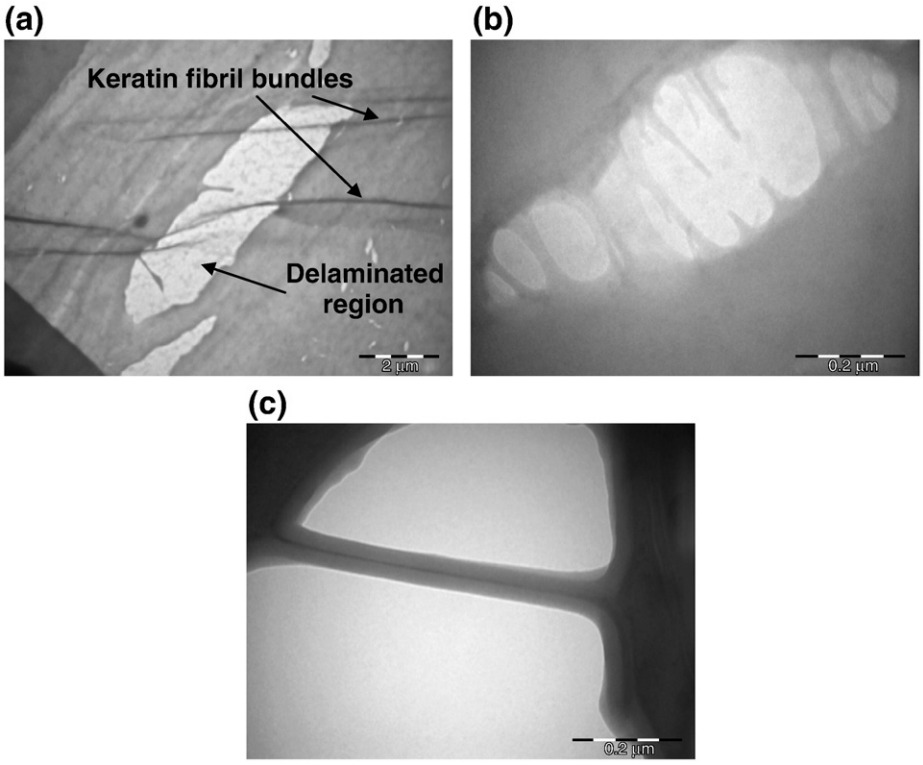

Fig. 5. TEM micrographs of a cross-section of sheep horn (longitudinal (growth) direction points out of page). (a) The large white region is a delaminated region between two lamellae, which has keratin fibril bundles embedded in both lamellae and stretching across the delaminated region (scale marker = 2 μm). (b) Numerous fibril bundles are observed across a delaminated region (scale marker = 200 nm). (c) The strongly diffracting crystalline keratin fibril bundle is surrounded by an amorphous matrix (scale marker = 200 nm).

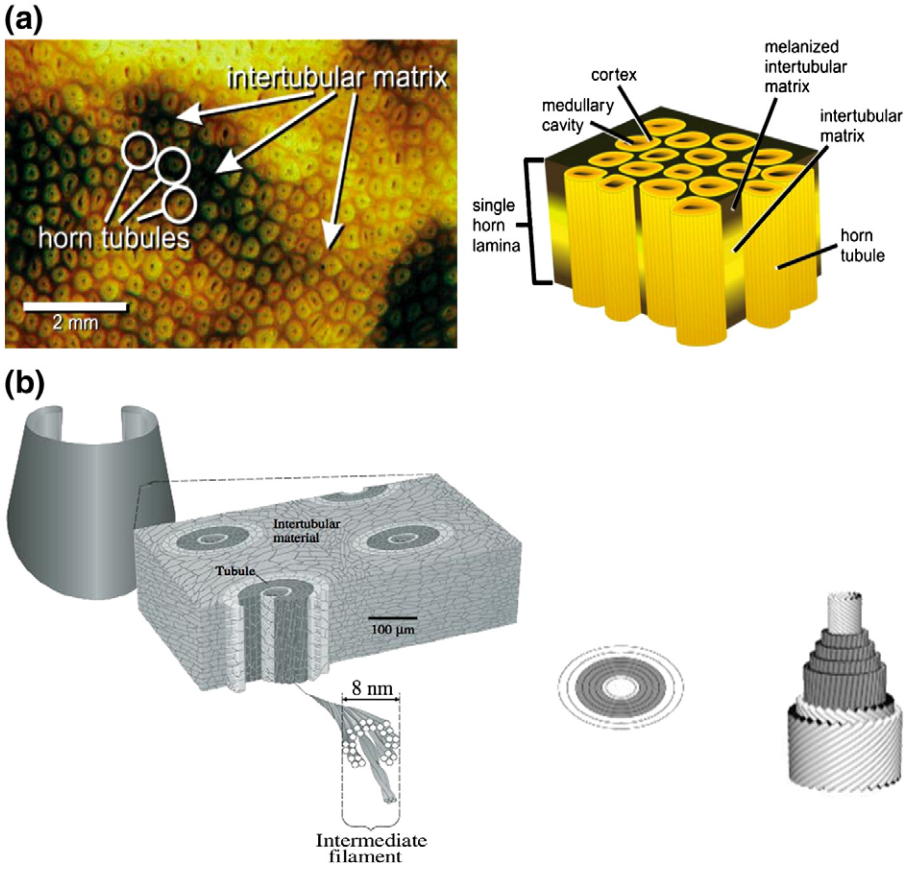

Fig. 6. (a) Tubule structure of the rhinoceros horn, taken from Hieronymus et al. [22] and (b) structure of an equine hoof. Keratin fibrils form hollow tubules. Taken from Kasapi and Gosline [30].

3.2.2. Hoof

Hooves are similar to horns and are composed of α-keratin fibers that are wound into circular lamellae that surround a hollow, empty channel, as shown in Fig. 6(b) [28–30]. Kasapi and Gosline [29,30] determined that the tubules only serve mechanical functions; they are not used to keep the hoof hydrated. A gradient of porosity exists through the thickness of the hoof wall with the highest density of tubules occurring at the outer surface and a lower density towards the inner part. However, the elastic modulus is highest at the outer surface, which does not correlate with a low tubule density, and is the result of an increase in the volume fraction of crystalline α-keratin filaments [28,30].

3.3. Comparisons

Table 1 lists the mineral fractions, densities and porosities of the examined mammalian structural materials. The outstanding feature is the presence of tubules that surround a medullary cavity (in the horn and hoof), osteons that surround blood vessels (bone) or hypermineralized tubules (teeth and tusks). The channel diameters of the tubules are very small for dentin (1 µm), larger for bone (~30 µm) with horn and hoof representing the largest values (up to 100 µm). The tubule density is very large for dentin (38,000 mm^{-2}) and is the smallest for the rhinoceros horn (7 mm^{-2}), with hooves, sheep horns, and bone falling in between these two values. The medullary cavity (or blood vessel diameter in bone) along with the tubule density can be used to calculate the amount of porosity. The porosities are within a small range, from 3% for the horse hoof to 12% for the dentin. The densities of the materials increase with increasing mineral content, which is to be expected since the density of the mineral (3.15 g/cm^3) is larger than that of the proteins (1.35 g/cm^3).

The Vickers hardness number (VHN) of each biological sample that we examined is listed in Table 2. The VHN progressively increases with mineral content, which was expected due to the high hardness of the mineral phase compared with the biopolymer matrix. The yield strength

Table 1
Dimensions of the microstructural features in mammalian structural materials.

Property	Horse hoof	Rhino horn	Sheep horn	Cancellous antler	Compact antler	Compact bovine femur	Dentin	Enamel
Mid-range tubule density (mm^{-2})	24 [31]	7[a]	22		36	16	38.000	
Channel diameter (µm)	40 [28]	100	40×100		25	30	1 [12]	
Porosity (%)	3[b]	6[b]	7		9	5	12	
Ash (%)				24 [7]	57 [7]	67 [32]	70	98 [19]
Mineral (vol.%)				24[c]	34[c]	44[c]	47 [33]	92[c]
ρ (g/cm^3)			1.2	0.5	1.72 [7]	2.06 [32]		3.08

[a] Estimated from micrograph in Ryder [33].
[b] Calculated from micrographs.
[c] Calculated from ash content, assuming that there is 10 wt.% water and all of the inorganic phase is collagen (density 1.35 g/cm^3).

Table 2
Vickers hardness number values and calculated yield strength, σ_y.

Source	Region	VHN (MPa)	σ_y (MPa)
Big horn sheep horn		145	48
Elk antler compact bone		202	67
Bovine compact bone		488[a]	163
Teeth	Dentin	500	167
	Enamel	1500	500

[a] Hodgekinson et al. [34].

Table 3
Comparison of the mechanical properties of mammalian structural biological materials.

	Compact bovine femur	Compact antler bone	Human dentin	Human enamel	Horse hoof	Sheep horn
Young's modulus (GPa)	13.5	7.8	17.6 [35]	80 [15]	0.4 [28]	2.4
Bending strength (MPa)	247	197	16.7 [10]		218–568	127
Strain to failure (%)						
Longitudinal	5	13.3			47 [28]	13.8
Transverse						>80
Impact energy (kJ/m^3)	5	14				20
Work of fracture (MJ/m^2)	1.7	13.9	0.270–0.550 [36]	0.013–0.200 [36]		30
Fracture toughness (MPa/m$^{1/2}$)	2–5 [7]	8–10 [7]	2.4 [37]	0.6–1.6 [38]		

can be related as approximately 1/3 of the VHN, which shows that the yield strength is expected to increase as the mineral fraction increases in these biological materials.

Table 3 lists the Young's modulus, strength, and toughness for the materials examined. These values represent samples loaded so that the main tensile load is along the growth direction (longitudinal direction). This is the direction along the osteons or tubules in these materials. Because antler bone has a lower mineral fraction than bovine femur, the antler bone has a Young's modulus that is 2× less than that of a bovine femur and a fracture toughness that is 2× as high. Dentin and enamel have higher mineral contents and consequently have a higher Young's modulus and a lower work of fracture. Hoof and horn have significantly lower Young's moduli and large strains to failure and horn has the highest work of fracture, compared to the mineralized materials.

In Fig. 7, SEM micrographs of the cross-sections of the elk antler, bovine femur, human tooth, and sheep horn show striking similarities. All show circular or elliptically shaped pores that are from the tubules aligning in the longitudinal direction. The size of the tubular structures in the femur and antler are the same — osteons are ~200 μm with vascular channels around 30 μm in diameter. The antler has a higher density of osteons, due to its relatively young age compared with the femur. The density of tubules in dentin is much higher than that of bone and the diameters are much less than that of bone — around 1 μm resulting in an areal porosity of 12%. The tubules in horn are elliptical ~40×100 μm, larger than that of bone or dentine. Hooves have a smaller porosity of 24 μm diameter and a much smaller porosity of ~3%. These micrographs provide evidence of the importance of tubules in an energy absorbent materials design. The tubules provide toughening mechanisms such as crack deflection, energy to collapse tubules, plus help prevent extended regions of microbuckling of the laminates.

One important characteristic in these structural biological materials is the effect of hydration. Bone, antler, and horn have a higher Young's modulus and higher yield strength in the dry condition compared to the rehydrated condition and consequently have a lower toughness. Water

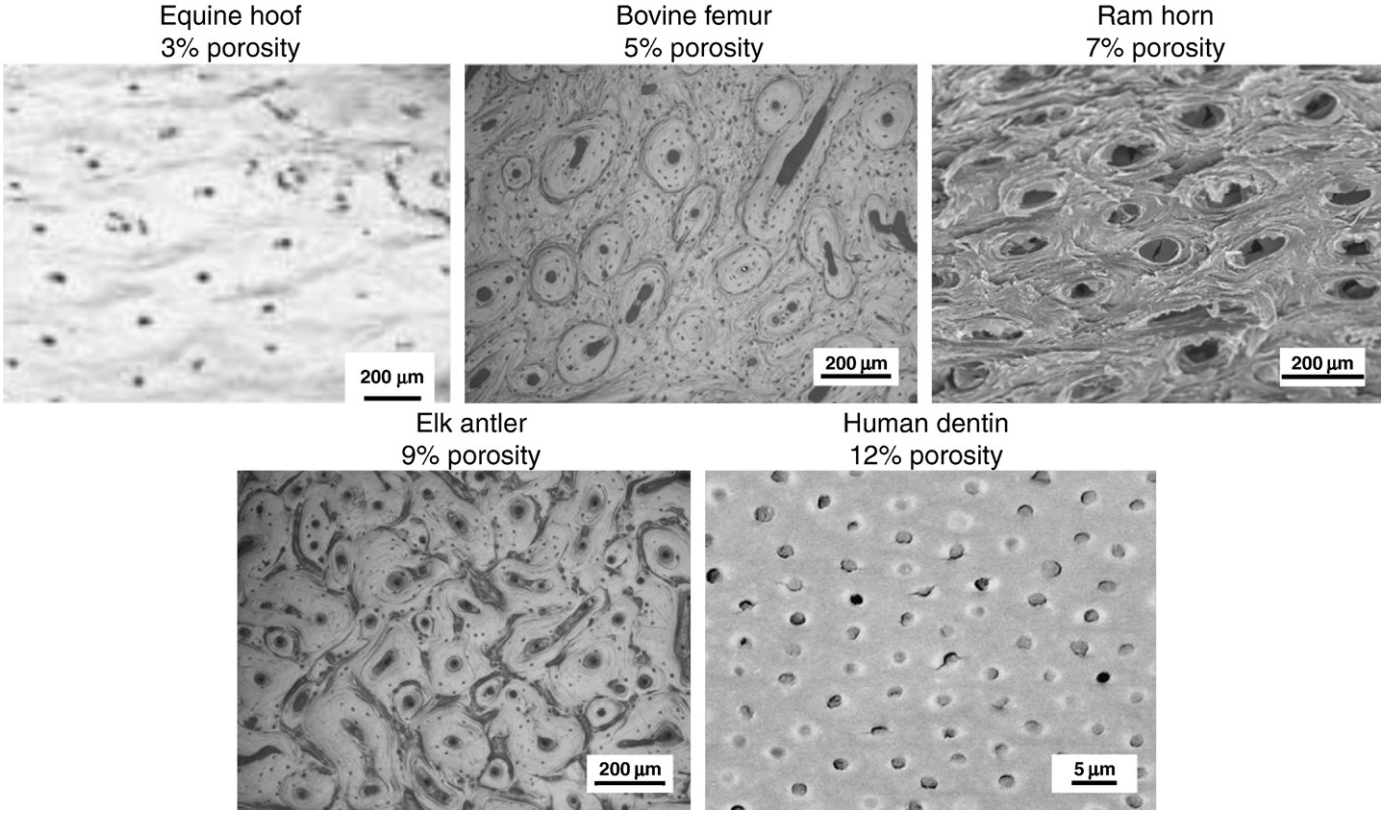

Fig. 7. Similarities between the transverse microstructures of hoof, bone, horn, antler and dentin. Growth direction points out of the page. The equine hoof micrograph was adapted from Kasapi and Gosline [28].

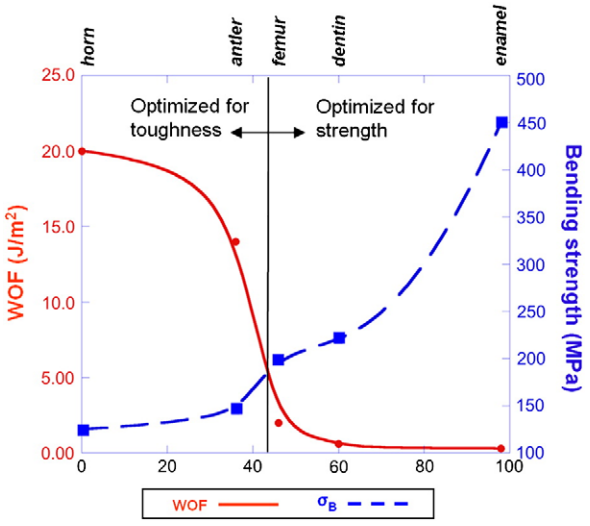

Fig. 8. Effect of mineralization on the work of fracture (WOF) and bending strength. Data taken from Chen et al. [7], Currey [32], Frank and Nalbandian [33] and Waters [12].

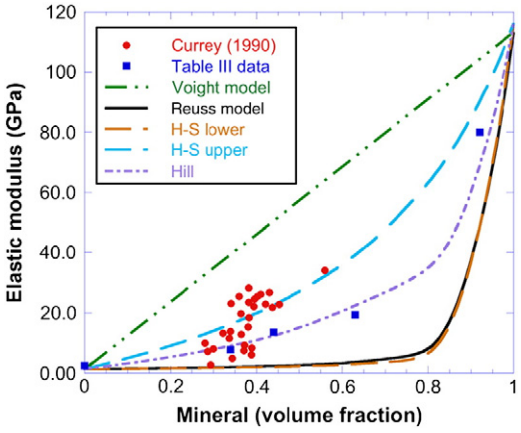

Fig. 9. Young's modulus as a function of mineral content for various mineralized biological materials. The curves are plotted from the Voigt (Eq. (5)), Reuss (Eq. (6)), lower and upper bounds from Hashin–Shtrikman (H–S) model (Eq. (10)) and the Hill model (Eq. (11)).
Data plotted from Currey [40] and from Table 3.

serves as a plasticizer in the horn keratin matrix but does not disrupt the keratin fibers [23,39]. In bone, water promotes more deformation of the collagen, but the exact mechanism of admitting more deformation remains unclear [10].

The effect of mineralization on the biopolymer shows that as the mineral fraction increases, the strength also increases but the work of fracture (WOF) decreases, as shown in Fig. 8. Plotted are the results from our work on bone, antler and horn (in bending) along with published data for bone, dentin and enamel [7,12,32,33]. From looking at the WOF curve, the horn has the highest value but a severe drop when the mineral content increases past ~35 vol.% and drops to nearly 0 at 100 vol.% mineral (near the value for enamel). In contrast, the bending strength increases as the mineral content increases, with horn owning the lowest strength and enamel owning the highest strength. Bone, at ~45 vol.% mineral content, is in the middle of the curves. Typically, high mineral content materials are optimized for strength while lower mineral content materials are optimized for WOF. The crossover between the bending strength and WOF occurs at the bone value, indicating that bone is optimized for both strength and toughness. The cost of increasing the strength of these materials is high in that the fracture resistance is severely sacrificed. This suggests that as the functional use of a biological material becomes more strictly dedicated to impact loading, the mineral content must be lowered. This is due to the brittle nature of hydroxyapatite; if too much is present, the composite acts as a brittle solid. This is what is found from synthetic particulate or fiber-reinforced polymers. The bending strength initially increases with increasing the fraction of the stronger brittle phase, then drops as the material starts behaving as a brittle solid, when the statistical distribution of flaws supercedes the theoretical strength of the brittle phase.

Fig. 9 shows a comparison of the Young's moduli (from Table 3) as a function of mineral content with the Voigt, Reuss, Hashin–Shtrikman and Hill models plotted with data from Currey [40]. The Voigt and Reuss averages provide upper and lower bound assessments for the effective elastic modulus of a polycrystalline material, respectively. They can also be used to estimate the effective elastic modulus of a composite elastic material. The Voigt (isostrain) model gives the elastic modulus as:

$$E_{\text{Voight}} = (1-f)E_1 + fE_2, \tag{5}$$

where E_1 is the elastic modulus of the collagen phase (1.3 GPa), E_2 is the elastic modulus of hydroxyapatite (116 GPa) and f is the volume fraction of the hydroxyapatite. The Reuss (isostress) model gives the elastic modulus as:

$$E_{\text{Reuss}} = \frac{1}{\frac{1-f}{E_1} + \frac{f}{E_2}}. \tag{6}$$

The best (narrowest) bounds for the effective elastic properties of polycrystalline materials are provided by the model of Hashin–Shtrikman, which defines the bulk (K) and shear (G) effective elastic moduli of a two-phase material as [41]:

$$K_{H\text{–}S_{\text{lower}}} = K_1 + \frac{f}{\frac{1}{K_2-K_1} + \frac{3(1-f)}{3K_1+4G_1}} \text{ and } K_{H\text{–}S_{\text{upper}}} = K_2 + \frac{1-f}{\frac{1}{K_1-K_2} + \frac{3f}{3K_2+4G_2}} \tag{7}$$

$$G_{H\text{–}S_{\text{lower}}} = G_1 + \frac{f}{\frac{1}{G_2-G_1} + \frac{6(1-f)(K_1+2G_1)}{5(K_1+4G_1)G_1}} \text{ and } G_{H\text{–}S_{\text{upper}}} = G_2 + \frac{1-f}{\frac{1}{G_1-G_2} + \frac{6f(K_2+2G_2)}{5(K_2+4G_2)G_2}} \tag{8}$$

where

$$K_i = \frac{E_i}{3(1-2\nu_i)} \text{ and } G_i = \frac{E_i}{2(1+\nu_i)}. \tag{9}$$

Here ν_i is the Poisson's ratio, taken as 0.2 for both the biopolymer (1) and mineral phase (2). The lower and upper bounds for the effective elastic modulus is:

$$E_{H\text{–}S_{\text{lower}}} = \frac{9K_{H\text{–}S_{\text{lower}}}G_{H\text{–}S_{\text{lower}}}}{3K_{H\text{–}S_{\text{lower}}} + G_{H\text{–}S_{\text{lower}}}} \text{ and } E_{H\text{–}S_{\text{upper}}} = \frac{9K_{H\text{–}S_{\text{upper}}}G_{H\text{–}S_{\text{upper}}}}{3K_{H\text{–}S_{\text{upper}}} + G_{H\text{–}S_{\text{upper}}}}. \tag{10}$$

Hill [42] suggested assessing the value of the effective elastic modulus as the mean average of the upper and lower Hashin–Shtrikman bounds:

$$E_{\text{Hill}} = \frac{E_{H\text{–}S_{\text{lower}}} + E_{H\text{–}S_{\text{upper}}}}{2}. \tag{11}$$

From Fig. 9 it can be seen that the Voigt and Reuss models grossly under- and overestimate the data, which indicates that simple composite models cannot be used to predict the elastic modulus. The upper bound of the Hashin–Shtrikman model more closely approximates the data, whereas the lower bound is still significantly

underestimates the values. The closest agreement is with the Hill model, where the data from Table 3 falls closely to the curve. It should be noted that all of the above-mentioned effective elastic parameter assessments are derived for an isotropic elastic material, while biological materials possess significant anisotropy. Given the anisotropy (presence of tubular structures, biopolymer fiber alignment) of the materials listed in Table 3, it is interesting that the Hill model adequately describes variation of the elastic modulus with mineral content. The data from Currey [40] are taken from bones from various taxa and our femur and antler bone data fall in Currey's range. However, we have extended the mineral volume fraction to include dentin and enamel, which have higher mineral contents than bone.

The nominal compression stress–strain behavior is shown in Fig. 10 (a) along with hysteresis curves (Fig. 10(b)) for horn (100% keratin) and demineralized antler (100% collagen). In Fig. 10(a), both materials show an initial elastic region followed by a plateau and then a final upturn, characteristic of nominal stress-strain curves. This upturn takes place after damage such as delamination and microbuckling has occurred and the tubules have collapsed. The peak stress, σ_p, (compressive yield strength) represents the maximum stress before densification occurs. Although it is higher for the horn than for antler, the specific strengths are similar (31.5 MPa for horn, 31.81 MPa for demineralized antler). Energy absorption of antler and horn can be largely attributed to the presence of the tubular structure and microdeformation mechanisms. Fig. 10(b) illustrates a large hysteresis in the stress–strain behavior for the horn compared with demineralized antler bone. The rehydrated horn and antler were loaded to the same peak load and then unloaded. The horn had a hysteresis loss of 5.48 MJ/m^3 compared with antler at 0.37 MJ/m^3. According to Vincent [43], in keratin the crystalline α-helices reform during unloading, with the amorphous keratin supporting the elastic load. This demonstrates that the horn is capable of dissipating large amounts of viscoelastic energy during deformation, acting like a shock absorber. The antler has a smaller hysteresis, likely due to the more elastic behavior of collagen fibers.

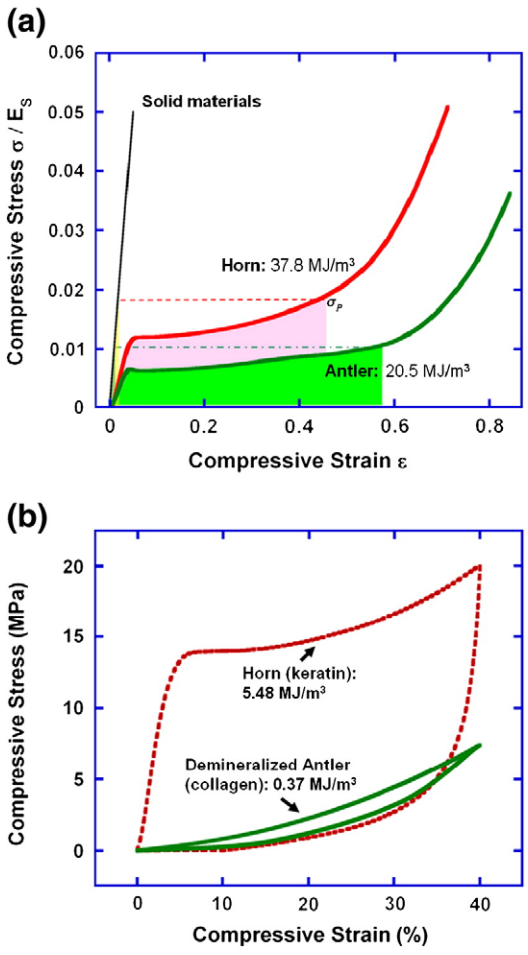

Fig. 10. (a) Nominal compressive stress-strain curves for horn and antler, compared to a completely dense bone. (b) Compressive hysteresis curves for horn and antler.

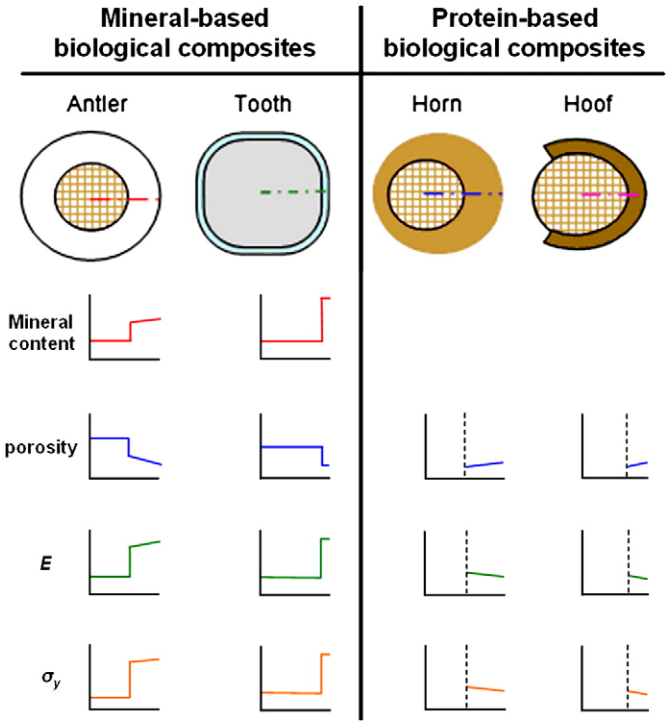

Fig. 11. Property and structural gradients across antler, tooth, horn, and hoof.

In Fig. 11, several material properties and structural feature gradients are plotted through the thickness for antler, tooth, horn and hoof. The protein-based materials (horn and hoof) have similar property and structural gradients, i.e., the elastic modulus porosity gradients and yield strength of horn and hoof follow the same trends through the thickness. The same is true for the mineral-based materials (antler and tooth). Comparing the mineral-based to the protein-based materials, all four of the materials follow reverse trends, with the exception of porosity. The elastic modulus is higher at the surface than at the core for the mineral-based materials, while the opposite is true for the protein-based materials. This is due to the higher mineral content at the surface for tooth and antler compared with the core. The commonality shared by each of the materials is that porosity is lowest at the surface. The low surface porosity may be important for these natural materials in order to prevent excess diffusion of water at the surface that could result in dehydration or over hydration of the material, thereby compromising the desired material properties.

As the porosity increases, the material is capable of higher energy absorption and has better fracture toughness. Porosity also decreases the structural weight; however, the tradeoff is lower strength. Mineral content is completely antagonistic to porosity. Increasing water content has a similar effect as increasing the porosity except that the water adds additional weight while porosity lessens the weight.

3.4. Bioinspired design strategies

The common themes from these studies are (1) presence of tubules, (2) a density gradient, (3) Young's modulus gradient, and (4) an amorphous polymer matrix reinforced by crystalline polymer fibers. There are several bioinspired designs that can be considered. One

possible design involves encasing a central porous core with an impact resistant polymer containing tubules oriented perpendicular to the loading direction. The central core should be made of a material with a higher elastic modulus than the material chosen for the outer sheath. However, the tubules and matrix materials comprising the outer sheath should have similar properties and very good adhesion.

4. Summary

Structural biological mammalian materials have surprising similarities in the microstructures. One overarching design similarity between bones, antlers, teeth, horns and hooves is the presence of multiple, distinct reinforcing layers, with outstanding energy absorption and unique deformation mechanisms. Additional similarities include a hierarchical structure and the presence of long tubules (vascular channels in the case of skeletal and bone) that extend in the longitudinal (growth) direction. The materials are also anisotropic, due to the presence of tubules and oriented structural protein fibers. Surrounding these tubules are circular lamellae that are assembled from strong, tough high aspect ratio crystalline protein fibers (collagen or keratin) that reinforce an amorphous protein matrix.

Despite the remarkable similarities shared by these materials, some differences do exist. The tubules within bones and teeth contain fluid, but no fluid is present in the hooves or horns. The tubules in hooves and horns have these mechanical functions: increasing the elastic hysteresis and energy absorption and also serving to prevent microbuckling of the lamellae. Because there is no mineralized component, these biological materials have a high toughness, but a low Young's modulus. In bones and teeth, additional reinforcement is achieved from nanocrystalline carbonated hydroxyapatite crystals, which have a platelet morphology with a large aspect ratio. This translates into a higher Young's modulus than what would be found from spherical particles. The biological composites have orders of magnitude higher toughness than a single phase mineral. Finally, for the mineralized tissues, since the mineral phase is nanocrystalline, it does not fracture, but strengthens the matrix. There is a high degree of interaction between the mineral phase and the biopolymer, an interlocking that is chemical and mechanical in nature, which strongly enhances the mechanical properties. Thus, the rule of mixtures cannot describe the mechanical properties of bones and teeth and grossly underestimates the properties. The Hashin–Shtrikman model provides a closer fit with the data but the Hill model adequately predicts the elastic modulus as a function of mineral content for samples taken from antler, bone, dentin and enamel.

The high-energy absorption of these biological materials can be attributed to microdeformation mechanisms such as delamination and microbuckling of the lamella. These deformation mechanisms are controlled primarily by the tubule distribution. Each lamella is composed of fibrous proteins that form the tough base material. This is the best design for energy absorption, which correlates with the functional use of these structural biological materials.

Bioinspiration does not result from the observations of natural structures alone but requires a thorough investigation of structure–function relationships in biological materials. Nature utilizes a number of strategies to create outstanding functional properties with comparatively inexpensive base materials. We have identified two strategies utilized in mammalian structural biological materials: mineral based and keratin based. Furthermore, we have quantified the effects of the most influential structural and environmental parameters. This work can serve as a foundation for engineering bioinspired composites.

5. Material sources

The antler (elk, *Cervus canadensis*) and horns (desert big horn sheep, *Ovis canadensis*) were either purchased from Into the Wilderness Trading Company, Pinedale, WY or donated by Montana, Fish, Wildlife and Parks. The antler, from a large, mature bull, was shed approximately one year before obtaining the antler for testing. The horn is approximately 7 years old (determined by counting the annular rings). The bovine femur, from an 18-month-old steer, was purchased from a local butcher. The teeth from the great white (*Carcharodon carcharias*) and mako (*Isurus oxyrinchus*) shark, and sawfish (*Pristis pectinata*) were donated by the Scripps Institute of Oceanography. Piranha (*Serrasalmus manueli*) and Amazon dogfish (*Rhaphiodon vulpinus*) teeth were from fish caught in Brazil. Rat (*Rattus norvegicus*) teeth were obtained from animals in the local fields around La Jolla. Human teeth were generously donated by Bruce Schwandt, D.D.S., Laguna Hills, CA.

Acknowledgements

We gratefully acknowledge support from Evelyn York (Scripps Institute of Oceanography) and Ryan Anderson (Nano3 Laboratory) for scanning electron microscopy, Prof. Paul Price and Damon Toroian (UCSD), Prof. John Skedros (University of Utah), Prof. Julian Vincent (University of Bath), Prof. Seong Jin Park (Center for Advanced Vehicular systems), and Dr. Matthew Tucker (Mississippi State University) for helpful discussions. This research was funded by the National Science Foundation, Division of Materials Research, Biomaterials Program (Grant DMR 0510138), the Army Research Office (Grant W911-08-1-0461), and a UC MEXUS-CONACYT Collaborative Grant. MFH and MWT would like to thank the Center for Advanced Vehicular Systems (CAVS) at Mississippi State University for supporting this work.

References

[1] U.G.K. Wegst, M.F. Ashby, Phil. Mag. 84 (2004) 2167.
[2] J. Henshaw, Nature 231 (1971) 469.
[3] L. Tombolato, E.E. Novitskaya, P.-Y. Chen, F.A. Sheppard, J. McKittrick, Acta Biomater. 6 (2010) 319.
[4] P.-Y. Chen, F.A. Sheppard, J.M. Curiel, J. McKittrick, Materials Research Society Symposium Proceeding, vol. 1132E, Fall 2008, Symposium Z1.4.
[5] M.E. Launey, P.-Y. Chen, J. McKittrick, R.O. Ritchie, Acta Biomater. 6 (2010) 1505.
[6] R.M. Kulin, P.-Y. Chen, F. Jiang, J. McKittrick, K.S. Vecchio, JOM 62 (2010) 41.
[7] P.-Y. Chen, A.G. Stokes, J. McKittrick, Acta Biomat. 5 (2009) 693.
[8] P.-Y. Chen, A.Y.M. Lin, Y.S. Lin, Y. Seki, A.G. Stokes, J. Peyras, E.A. Olevsky, M.A. Meyers, J. McKittrick, J. Mech. Behav. Biomed. Mater. 1 (2008) 208.
[9] J.D. Currey, in: J.G. Carter (Ed.), Skeletal Biomineralization: Patterns, Processes and Evolutionary Trends I, Van Nostrand Reinhold, New York, 1990, p. 11.
[10] J.D. Currey, Bones: Structure and Mechanics, Princeton University Press, Princeton, NJ, 2002, p. 127.
[11] S. Weiner, H.D. Wagner, Ann. Rev. Mater. Sci. 28 (1998) 271.
[12] N.E. Waters, in: J.F.V. Vincent, J.D. Currey (Eds.), The Mechanical Properties of Biological Materials, Symp. Soc. Exp. Biol., vol. 34, Cambridge University Press, Cambridge, 1980, p. 99.
[13] M.L. Snead, D. Zhu, Y. Lei, S.N. White, C.M. Snead, W. Luo, M.L. Paine, Mater. Sci. Eng. C 26 (2006) 1296.
[14] V. Imbeni, R.K. Nalla, C. Bosi, J.H. Kinney, R.O. Ritchie, J. Biomed. Mater. Res. A 6 (2003) 1.
[15] L.H. He, N. Fujisawa, M.V. Swain, Biomaterials 27 (2006) 4388.
[16] R. Garberoglio, M. Brännstrom, Arch. Oral Biol. 21 (1976) 355.
[17] U. Schellenberg, G. Krey, D. Bosshardt, P.N.R. Nair, J. Endodont. 18 (1992) 104.
[18] I.A. Mjör, I. Nordahl, Arch. Oral Biol. 41 (1996) 401.
[19] J.H. Kinney, M. Balooch, G.W. Marshall, S.J. Marshall, Arch. Oral Biol. 44 (1996) 813.
[20] H. Cezayirlioglu, E. Bahniuk, D.T. Davy, K.G. Heiple, J. Biomech. 18 (1985) 61.
[21] H. Gao, B. Ji, I.L. Jäger, E. Arzt, P. Fratzl, PNAS 100 (10) (2003) 5597.
[22] T.L. Hieronymus, L.M. Witmer, R.C. Ridgely, J. Morph. 267 (2006) 1172.
[23] A. Kitchener, J.F.M. Vincent, J. Mater. Sci. 22 (1987) 1385.
[24] L.M. Kachanov, Delamination buckling of composite materials, Kluwer Academic Publishers, The Netherlands, 1988, p. 19.
[25] R. Menig, M.H. Meyers, M.A. Meyers, K.S. Vecchio, Acta Mater. 48 (2000) 2383.
[26] A. Morales, Proc. 22nd Int. SAMPE Tech. Conf, Nov. 6–8 1990, p. 1217.
[27] K. Dransfield, C. Baille, Y.-W. Mai, Comp. Sci. Tech. 50 (1994) 305.
[28] M.A. Kasapi, J.M. Gosline, J. Exp. Biol. 200 (1997) 1639.
[29] M.A. Kasapi, J.M. Gosline, Equine Vet. J. 26 (1998) 10.
[30] M.A. Kasapi, J.M. Gosline, J. Exp. Biol. 202 (1999) 377.
[31] J.D. Reilly, S.N. Collins, B.C. Cope, L. Hopegood, R.J. Lathan, Equine Vet. J. 26 (Suppl) (1998) 4.
[32] J.D. Currey, J. Biomech. 12 (1979) 313.
[33] R.M. Frank, J. Nalbandian, in: A. Oksche, L. Vollrath (Eds.), Teeth, Springer-Verlag, Berlin, 1989, p. 173.
M.L. Ryder, Nature 193 (1962) 1199.
[34] R. Hodgskinson, J.D. Currey, G.P. Evans, J. Ortho. Res. 7 (5) (1989) 754.

[35] R.G. Craig, F.A. Peyton, J. Dent. Res. 37 (4) (1958) 710.
[36] S.T. Rasmussen, R.E. Patchin, D.B. Scott, A.H. Heuer, J. Dent. Res. 55 (1976) 154.
[37] J. Yan, K.B. Clifton, J.J. Mecholsky Jr., R.L. Reep, J. Biomech. 39 (2006) 1066.
[38] H.H. Xu, D.T. Smith, S. Jahanmir, E. Romberg, J.R. Kelly, V.P. Thompson, E.D. Rekow, J. Dent. Res. 77 (1998) 472.
[39] A. Kitchener, J. Mater. Sci. Lett. 6 (1987) 321.
[40] J.D. Currey, J. Biomech. 23 (1990) 837.
[41] Z. Hashin, S. Shtrikman, J. Mech. Phys. Solids 11 (1963) 127.
[42] R. Hill, J. Mech. Phys. Solids 13 (1965) 213.
[43] J. Vincent, Structural Biomaterials, Revised Edition, Princeton University Press, Princeton, NJ, 1990.